Whining noise computation of a planetary gear set induced by the multi-mesh excitations

Jessica Neufond, Enora Denimal, Emmanuel Rigaud, Joël Perret-Liaudet, Alexandre Carbonelli

Journal Title
XX(X):1–10

DOI: 10.1177/ToBeAssigned
www.sagepub.com/

Whining noise computation of a planetary gear set induced by the multi-mesh excitations

Jessica Neufond[1,2], Enora Denimal[1], Emmanuel Rigaud[1], Jöel Perret-Liaudet[1], Alexandre Carbonelli[2]

Abstract

A complete procedure for the whining noise computation of a planetary gear set induced by the multi-mesh excitations is presented. This procedure is divided into three main steps. First, the parametrical internal excitations are simultaneously characterized by considering all contacts at the multiple gear meshes. Secondly, a finite element model of the planetary gear set is built. Finally, the coupled equations of motion are projected onto the modal basis and the stationary dynamic response is computed using an iterative spectral method.

Keywords

Planetary gear, mesh stiffness fluctuation, static transmission error, dynamic transmission error, dynamic mesh force, housing vibration

Introduction

Planetary gear systems provide high gear ratio in a compact package. They are used for example in automatic gearboxes, transmissions for hybrid vehicles, energy production systems such as wind turbines, home automation applications such as shutters and blinds.[1] The vibroacoustic behaviour of planetary gear sets has to be considered closely in the design process. Contrary to cylindrical gears with fixed and parallel axes, predicting and controlling the whining noise remain a difficult problem because of the coupling between the multiple gear meshes and the mobility of the planets axes. It is assumed that the gear whining noise is generated by the mesh process, including parametric internal excitations. Static Transmission Error (STE) and gear mesh stiffness fluctuations generate dynamic mesh forces which are transmitted to the housing through wheel bodies, shafts and bearings.[2–4] The housing vibratory state is directly related to the radiated noise.[3;4]

STE corresponds to the difference between the actual position of the driven gear and its theoretical position for a very slow rotation velocity and for a given applied torque.[2;3] It results from teeth deflections, teeth surface modifications and manufacturing errors. For cylindrical gears with fixed and parallel axes, the computation of the STE under static mesh load is well mastered.[5;6] It is based on the resolution of the equation describing the static contact between the gear teeth. In the case of planetary gear sets, the power transmission combines several sun gear/planet and planet/ring gear meshes which are coupled to each other. Therefore, load distribution between each contact zone depends of the whole system deformation, the initial distance between tooth surfaces and the position errors of solids.[7–10]

In the context of dynamic modelling, the main excitations are generally introduced as a combination of periodic displacement excitations and periodic mesh stiffness fluctuations (parametric excitation). The equations of motion are coupled because of the different gear meshes. For current geared systems whose discretized models present a large number of degrees-of freedom, computation time may become a problem. Some authors try to minimize computation time by using lumped-parameters models[11] or hybrid models.[12] Hybrid models are the combination between lumped-parameter models and finite element models of some flexible components (usually the ring gear and the planet carrier). These models remain sufficiently accurate while reducing the size of the problem to be solved. An alternative method has been proposed.[13;14] The iterative spectral method allows the solving of linear parametric equations of motion in the spectral domain with short computational time. Its effectiveness has been demonstrated for predictions and analyses of the dynamic response and whining noise for single,[13;14] and multi-gears systems such as planetary gear sets.[15]

This paper proposes a complete procedure using a finite element modelling of the planetary gear set and the computing of the stationnary dynamic response induced by the parametric excitations and their coupling. In a first step, the main internal excitations are simultaneously

[1]Laboratoire de Tribologie et Dynamique des Systèmes LTDS UMR 5513, Univ Lyon, Ecole Centrale de Lyon, ENISE, ENTPE, CNRS, 36 avenue Guy de Collongue, F-69134, ECULLY, France
[2]Vibratec, 28 chemin du petit bois CS 80210, F-69134 ECULLY CEDEX, France

Corresponding author:
Jessica Neufond
Email: jessica.neufond@vibratec.fr

characterized by considering all the contacts at the multiple gear meshes. Therefore, both tooth deflection and tooth micro-geometries (voluntary profile modifications and manufacturing errors) are considered. The static equilibrium of the planetary gear is computed for a set of successive positions of the sun gear, in order to estimate static transmission error fluctuations. Gear mesh stiffness fluctuations are deduced from numerical derivative of input torque relative to STE. In a second step, the planetary gear set is modelled using the finite element method in order to compute its modal basis. In a third step, the coupled equations of motion are projected onto the modal basis and the stationary dynamic response is computed for any degree of freedom of the discretized model using an iterative spectral method.[13;15] Finally, the emitted sound power level is evaluated from the mean square velocity of the radiating surface of the housing following Rigaud and al.[16] works.

Description of the planetary gear set

The studied planetary gear set is a standard one used for several industrial applications. It is designed with one stage and three planets. Its main characteristics are given in Table 1. The input is the sun gear and the output is the planet carrier, letting the ring gear fixed. The gear ratio is:

$$\frac{\omega_c}{\omega_s} = \frac{Z_s}{Z_s + Z_r} = 0.2$$

with ω_c and ω_s the rotational speed of the carrier and the sun-gear, respectively, Z_s and Z_r the number of teeth of the sun gear and the ring gear, respectively.

Table 1. Main characteristics of the planetary gear

Parameters			
Data	Sun	Planets	Ring
Number of teeth	27	40	108
Module (mm)		1.5	
Pressure angle (deg)		20	
Helix angle (deg)		0	
Addendum coefficient		1	
Dedendum coefficient		1.25	
Center distance (mm)		50.8	

The planetary gear set is mounted on a test bench for incoming measurements of its dynamic behaviour (see Figure 1).

The input velocity is driven by an electric motor and the output torque is applied by a similar electric motor used as a brake. Motors and planetary gear set are connected by mechanical couplings. The input range speed is [0-3000 rpm] and the output torque range is [0-100 N.m]

[Insert Figure 1 (TestBench.eps)]

Computation scheme

Analysis of phase difference between meshes

Some authors have considered phase relationship between meshes of planetary gear set.[7;17;18]. Their works focus on the load sharing. However, even if they do not explicitly address the case of static transmission errors and mesh stiffness fluctuations, the procedure is similar and is the following. A planet is chosen as a reference. The remaining $(N-1)$ planets are shifted by $2\pi n/N$ with respect to the reference, where $n \in [1, \ldots, N]$. The $2N$ meshes are noted as follows: the planet number n meshes with the sun gear through the mesh number n and with the ring gear through the mesh number $(n+N)$. Finally, meshes are indexed by $j \in [1, \ldots, 2N]$.

For a given length h_1 on the reference action plane, the problem consists in finding the length h_n on the n^{th} sun/planet action plane. The angular position between the reference mesh and the n^{th} mesh is equal to $(2\pi n/N + \gamma_n)$, with:

$$\gamma_n = \frac{2\pi}{Z_s}\, modulo(\frac{2\pi}{3}) \tag{1}$$

The angle γ_n represents the length h_n on the n^{th} action plane equal to :

$$h_n = r_{bs}\gamma_j \tag{2}$$

where r_{bs} is the basis radius of the sun gear.

The phase between the planets and the ring gear is presented in Figure 2. It displays the planet n of center O_p which simultaneously meshes with the sun gear and the ring gear. The following notation is used:

- T_s is the contact point between the basis radius of the planet and the action line related to the sun gear. T_r is similarly defined for the ring gear.
- C_s and C_r are the contact points between the planet and the sun gear, and between the planet and the ring gear, respectively.
- $l_s = [T_s C_s]$ is the abscissa of contact between the sun and the planet. $l_r = [T_r C_r]$ is the abscissa of contact between the planet and the ring gear and must be determined.
- A_s and A_r are the intersections between the basis circle and the tooth flank involved in the mesh with the sun gear and the ring gear, respectively.

The problem to solve consists in the determination of the distance l_r knowing l_s. Under the hypothesis of an involute geometry with no clearance, it consists in determining a set of angles represented in Figure 2:

[Insert Figure 2]

- $\phi_s = \widehat{A_s O_p T_s}$
- $\phi_r = \widehat{A_r O_p T_r}$
- $\tau = \widehat{T_s O_p T_r}$,
- ψ: the angle of the tooth thickness on the basis circle
- κ : the angle between the tooth flank involved in the mesh with the sun gear and the ring gear, respectively.

Assuming that :

$$\phi_s = \frac{l_s}{r_{bp}} \tag{3}$$

where r_{bp} is the basis radius of the planet. The angle of the tooth thickness on the basis circle is equal to:

$$\psi = \frac{s}{r_b} + 2(\, tan(\alpha) - \alpha) = \frac{s}{r_b} + 2\, inv(\alpha) \tag{4}$$

where s is the circonferential thickness of the tooth at the basis circle and α is the pressure angle. Then, the angle between the two tangent points is equal to:

$$\tau = \pi - 2\alpha \tag{5}$$

κ is given by:

$$\kappa = \mathrm{E}(\frac{Z_p}{2})\frac{2\,\pi}{Z_p} \tag{6}$$

where E is the integer part function and Z_p the number of teeth of the planet.

Finally, the angle ϕ_r is equal to:

$$\phi_r = \psi + \kappa - \tau - \phi_s \tag{7}$$

and then:

$$_r = r_b\, \phi_r \tag{8}$$

Characterization of the static transmission errors and the mesh stiffness fluctuations

This part is devoted to the theoretical formulation of the calculation of the STE of a planetary gear. First, the formulation for a single mesh is presented before being extended to the case of the multimesh planetary gear.

For each angular position θ of the driving wheel, a kinematical analysis of the mesh allows determination of the theoretical contact lines on the tooth surfaces. The resolution of the contact equation leads to the evaluation of the STE $\delta(\theta)$ and the load distributio $\boldsymbol{P}$ along the contact lines. Hence, the contact equations are given by:[5]

$$\left\{ \begin{array}{c} \mathbf{H}.\boldsymbol{P} = \delta(\theta).\boldsymbol{1} - \boldsymbol{e} \\ {}^t\boldsymbol{1}.\boldsymbol{P} = \mathrm{F} \end{array} \right. \tag{9}$$

under the constraints:

$$\left\{ \begin{array}{c} -\mathbf{H}.\boldsymbol{P} + \delta(\theta).\boldsymbol{1} \leq \boldsymbol{e} \\ \mathrm{P}_i \geq 0 \end{array} \right. \tag{10}$$

where :

- $\mathbf{H}$ is the compliance matrix related to the nodes of discretized contact lines. It is a linear combination of each tooth wheel compliance matrix, computed previously by a finite element method,
- $\boldsymbol{P}$ is the vector of the load distribution on the contact line and P_i is the load on the i^{th} point of the contact line,
- $\delta(\theta)$ is the STE. It corresponds to the linear displacement of the gear related to the pinion along the line of action. This displacement is identical for all nodes of the contact line,
- $\boldsymbol{e}$ is the vector of initial gaps determined from the tooth surface modifications and manufacturing errors,
- F is the mesh static load induced by the input torque.

The STE is calculated for a set of successive position θ of the driving wheel, in order to evaluate its periodic time evolution.

In the case of planetary gear set with N planets, equations of contact are solved taking into account all the meshes simultaneously. In addition to the usual assumptions defined in previous works for gears with parallel and fixed axes[5;14], a rigid carrier with a purely rotational motion around its theoretical axis is assumed. Furthermore, perfect pivot joints with planets are assumed. Finally, for each planet, $\boldsymbol{\Delta}$ is defined as the sum of sun gear/planet STE and planet/ring gear STE, so that:

$$\Delta = \delta_1 + \delta_4 = \delta_2 + \delta_5 = \delta_3 + \delta_6 \tag{11}$$

Where δ_1, δ_2 and δ_3 refer to sun gear/planet STE, δ_4, δ_5, δ_6 to planet/ring gear ones.

The computation of each STE δ_j and each load distribution vectors $\boldsymbol{P}^{(j)}$ requires to minimize:

$$\boldsymbol{E}_j = \frac{1}{2}{}^t\boldsymbol{P}_j.\mathbf{H}_j.\boldsymbol{P}_j + \frac{1}{2}{}^t\boldsymbol{P}_j.\boldsymbol{e}_j - \frac{1}{2}F_j.\delta_j \tag{12}$$

under the constraints:

$$\left\{ \begin{array}{c} {}^t\boldsymbol{1}.\boldsymbol{P}_j = \mathrm{F}_j \\ \mathbf{H}_j.\boldsymbol{P}_j + \delta_j.\boldsymbol{1} \leq \boldsymbol{e}_j \\ P_{i,j} \geq 0 \\ \delta \geq 0 \end{array} \right. \tag{13}$$

where $\mathbf{H}_j$ is the compliance matrix, $\boldsymbol{e}_j$ are the initial gaps and F_j the transmitted load of the mesh j.

Hence, the computation of Δ corresponds to the minimization of the global energy given by :

$$\boldsymbol{E} = \sum_{j=1}^{2N} \boldsymbol{E}_j = \sum_{j=1}^{2N} (\frac{1}{2}{}^t\boldsymbol{P}_j.\mathbf{H}_j.\boldsymbol{P}_j + \frac{1}{2}{}^t\boldsymbol{P}_j.\boldsymbol{e}_j - \frac{1}{2}F_j.\delta_j) \tag{14}$$

under the contact constraints previously identified.

The input load F_T is transmitted by the sun gear to the N planets and then from the N planets to the ring gear, so that:

$$F_T = \sum_{n=1}^{N} F_n \tag{15}$$

$$F_T = \sum_{n=N+1}^{2N} F_n \tag{16}$$

And each planet transmits to the ring gear the totality of the load received from the sun gear, so that:

$$F_n = F_{n+N}\ ,\ \text{for } n \in [1, \ldots, N] \tag{17}$$

Using equations (11), (15) and (17) into equation (14), it comes:

$$\boldsymbol{E} = \sum_{j=1}^{2N} \left(\frac{1}{2} {}^{t}\boldsymbol{P}_j . \mathbf{H}_j . \boldsymbol{P}_j + \frac{1}{2} \boldsymbol{e}_j . \boldsymbol{P}_j \right) - \frac{1}{2} F_T . \Delta \qquad (18)$$

and for each set of parameters $(\mathbf{H}_j, \boldsymbol{e}, F_T)$, the unknown parameters $\boldsymbol{P}_j$ and δ_j are minimized using an interior-point-convex quadratic algorithm.

Otherwise, for each successive angular position θ of the driving wheel, the mesh stiffness $k_j(\theta)$ is defined as the derivative of the transmitted load F_j over the STE δ_j:

$$k_j(\theta) = \frac{\partial F_j}{\partial \delta_j(\theta)} \qquad (19)$$

The mean values of the mesh stiffness's are lately introduced in the finite elements model of the planetary gear set in order to compute its modal basis.

Modelling the planetary gear set and computing the modal basis

A finite element model of the planetary gear set is built and displayed in Figure 3. All the components (shafts, bodies) are modelled with 3D elements. The following assumptions are made:

- a rotating reference frame is attached to the carrier,
- the ring housing and its boundary conditions are axisymmetric, so that the modal basis doesn't depend on planet position during operation.

The elastic coupling between gears is modelled by introducing the mean value of the mesh stiffness's computed in the previous section. The sun gear is connected to the motor inertia through a torsional stiffness modelling the input mechanical coupling. The carrier shaft is connected to the brake inertia through a torsional stiffness modelling the output mechanical coupling. The boundary conditions of the planetary gear set connection with the test bench is assumed infinitely stiff.

[Insert Figure 3]

Centrifugal forces at the planets occur because of carrier rotation. They can have an impact on the dynamic response. Thanks to the finite element software NX Nastran ©, the centrifugal effects can be directly included in the finite element model. The principle is the following: a first simulation is performed in order to evaluate the modified stiffness matrix of the system caused by centrifugal forces. This new stiffness matrix is then transmitted to the modal analysis solver. This results in a modal basis depending on input rotational speed. For a proper simulation, a modal basis should be attached at each relevant speed step for the dynamic response computation procedure.

The centrifugal forces are evaluated for the studied system. First, two modal basis are compared. A first one for a low sun gear speed, and a second one for a sun gear speed equal to 3000 rpm (maximum speed allowed by the planetary gear set). Very low difference is observed: eigenfrequencies evolution is less than 1 Hz. Planets displacement is less than 1 μm. Furthermore, simulations show no influence on dynamic results. These results are relevant with the stiff system studied. Finally, centrifugal forces are neglected for the studied case to avoid long unnecessary computational steps. In the general case, one should be careful about taking or not taking into account these forces in the modal basis simulation depending on the whole system stiffness and the input rotation speed.

Finally, the modal basis is computed on the frequency range [0-10 kHz] and 117 modes are extracted.

Energetic contribution of the eigenmodes

An energetic approach allows identification of critical modes by comparing the local potential energy associated with the mesh stiffness with the full potential energy of the system.[19] Thus, an energy rate is defined for each mode and each mesh:

$$\mathbf{U}_{\mathbf{m}}^{(\mathbf{k})} = \frac{1}{2} (\phi_{\mathbf{j}}^{\mathbf{T}} [\mathbf{K_m}] \phi_{\mathbf{j}}) \qquad (20)$$

$$\mathbf{U}_{\mathbf{T}}^{(\mathbf{k})} = \frac{1}{2} (\phi_{\mathbf{j}}^{\mathbf{T}} [\mathbf{K_T}] \phi_{\mathbf{j}}) \qquad (21)$$

$$\rho_m^k = \frac{\mathbf{U}_{\mathbf{m}}^{(\mathbf{k})}}{\mathbf{U}_{\mathbf{T}}^{(\mathbf{k})}} \qquad (22)$$

where $\mathbf{K_m}$ is the local stiffness matrix associated with the mesh stiffness and $\mathbf{K_T}$ is the global stiffness matrix. This analysis allows identification of modes whose excitation generates an amplification of the dynamic response.

Computation procedure for the stationary response: an iterative spectral approach

For an axisymmetric ring gear, the equations of motion can be written as:

$$\mathbf{M}\ddot{\boldsymbol{x}} + \mathbf{C}\dot{\boldsymbol{x}} + \left[\mathbf{K} + \sum_{j=1}^{m} k_j(t) \boldsymbol{R}_j \boldsymbol{R}_j^T \right] (\boldsymbol{x}\text{-}\boldsymbol{x}_s) = \mathbf{0} \qquad (23)$$

With $\mathbf{M}$ and $\mathbf{K}$ the mass and stiffness matrices from the finite element model and $\mathbf{C}$ the damping matrix taken into account a posteriori through the Basile hypothesis. $\boldsymbol{R}_j$ is the structural vector that couples the wheel, $\boldsymbol{R}_j \boldsymbol{x}^T$ is the dynamic transmission error and $\boldsymbol{R}_j^T \boldsymbol{x}_s$ the static transmission error. The use of time discretization methods leads to prohibitive calculation times as a discretization over a long period is required for low frequency excitation, when a fine time step is required for high-frequency excitation. So that, parametric equations of motion are solved using the iterative spectral method, allowing the resolution of large systems of periodic differential equations with very short computation times. This method is based on the direct computation of the solution in the spectral domain.[13] To this end, the matrix equation 23 is rewritten in the mean modal basis with $\boldsymbol{x} = \mathbf{V}\boldsymbol{q}$:

$$diag[1]\ddot{\boldsymbol{q}} + diag[2\zeta_k\Omega_k]\dot{\boldsymbol{q}} + diag[\Omega_k^2]\boldsymbol{q} + \sum_{j=1}^{m} g_j(t)\boldsymbol{r}_j\boldsymbol{r}_j^T\mathbf{q} = \sum_{j=1}^{m} k_j(t)\boldsymbol{r}_j\boldsymbol{r}_j^T\boldsymbol{q}_s \quad (24)$$

where $\boldsymbol{q}$ is the modal co-ordinates vector, $\boldsymbol{r}_j = \mathbf{V}^T\boldsymbol{R}_j$ is the modal structural vector at the j^{th} mesh, Ω_k is the k^{th} natural frequency, ζ_k is the corresponding modal viscous damping, $g_j(t) = k_j(t) - \overline{k_j}$ is the fluctuating part of mesh stiffness's. The dynamic transmission errors $e_j(t) = r_j^T q$ and the static ones $\delta_j(t) = r_j^T q_s$ are introduced, the matrix equation 24 become in an indicial form:

$$\ddot{q}_k + 2\zeta_k\Omega_k\dot{q}_k + \sum_{j=1}^{m} g_j(t)r_{jk}e_j(t) = \sum_{j=1}^{m} k_j(t)r_{jk}\delta_k(t) \quad (25)$$

To solve equation 25, we introduced an iterative process directly achieved in the spectral domain. Retaining the stationary terms, the Fourier transform leads to:

$$H_k^{-1}(\omega)Q_k(\omega) + \sum_{j=1}^{m} G_j(\omega)r_{jk} \otimes E_j(\omega) = \sum_{j=1}^{m} K_j(\omega) \otimes r_{jk}\Delta_j(\omega) \quad (26)$$

with $H_k(\omega) = [(\omega_k^2 - \omega^2 + 2i\zeta_k\omega_k\omega)]^{(-1)}$. The operator $\otimes$ denotes the convolution product. In equation 26, $Q_k(\omega)$, $G_j(\omega)$, $E_j(\omega)$, $K_j(\omega)$ and $\Delta_j(\omega)$ are respectively the Fourier transforms of q_k, $g_j(t)$, $e_j(t)$, $k_j(t)$ and $\delta_j(t)$.

After several transformations, the iterative process can be written as follows:

$$E_i^{n+1}(\omega) = E_i^{(0)}(\omega) - \sum_{j=1}^{m} T_{ij}(\omega).[G_j \otimes E_j^{(n)}](\omega) \quad (27)$$

where $T_{ij}(\omega) = \sum_{j=1}^{m} T_{ij}(\omega).[K_j \otimes \Delta_j^{(n)}](\omega)$ is a scalar function which only depends on the modal characteristics. Initial solutions are:

$$E_i^{(0)}(\omega) = \sum_{j=1}^{m} T_{ij}(\omega).[K_j \otimes \Delta_j^{(n)}](\omega). \quad (28)$$

The convergence is tested from the relative difference between two iterations which is compared to a very small value ϵ, typically $\epsilon = 10^{-6}$.

$$\frac{||E_j^{n+1}(\omega) - E_j^n(\omega)||}{||E_j^{n+1}(\omega)||} < \epsilon \quad (29)$$

Another stop criterion is based on a maximal number of iterations beyond which divergence of the iterative scheme is assumed. This situation is due to possible parametric instabilities associated with the free response of the system.

Finally, the vibratory state of the system can be evaluated at any chosen point and any degree of freedom of the discretized model by a projection of the response on the modal basis.

Dynamic response of the housing

The aim of this section is to compute the dynamic response of the housing in order to simulate the signal measured by an accelerometer fixed on the ring gear. This accelerometer experiences modulation induced by the rotation of the carrier and the periode passage of the planets. Inapolat and al.[20] presented an analytical method to characterize the modulation sidebands induced by the rotating carrier. Following the proposed procedure[20], the progressive evolution and the passage of the planets in front of the accelerometer is simulated by a Hanning windowing function combined with Heaviside unit functions. Finally, the acceleration on the housing can be expressed as:

$$a(t) = \sum_{n=1}^{N} A_n(t)w(t - \frac{\Gamma_n}{\omega_c})U_n(t) \quad (30)$$

where:

$$w_n(t) = \frac{1}{2} - \frac{1}{2}\left[\cos(N\omega_c t)\right] \quad (31)$$

is the Hanning windowing function, and:

$$U_n(t) = \sum_{j=1}^{\infty} \left\{ \begin{array}{c} H\left[t - (\frac{(j-1)N+n-1}{N})T_c\right] - \\ H\left[t - (\frac{(j-1)N+n}{N})T_c\right] \end{array} \right\} \quad (32)$$

is the windowing function simulating the passage of planet n in front of the housing point,

with:

- $A_n(t)$ the time signal acceleration computed with the iterative spectral method, attached to planet n localization
- ω_c is the angular velocity of the carrier with respect to the inertial frame,
- N is the number of planets,
- Γ_n is the angular position of planet n,
- T_c is the revolution period of the carrier,
- $H(x)$ is the Heaviside unit step function ($H(x) = 1$ if $x > 0$ or $Hx) = 0$)

Whining noise radiated by the planetary gear set

The whining noise is directly related to the vibratory state of the geared system[16]. The sound power level radiated by the housing of a gear transmission is equal to:

$$W_{ac}(\omega) = \rho_0.c_0.S.\sigma_{rad}(\omega). < \overline{v^2(\omega)} > \quad (33)$$

where:

- ρ_0 is the air density,
- c_0 is the speed of sound in the air,
- S is the surface of the housing that radiates,
- $\sigma_{rad}(\omega)$ is the radiation factor of the housing depending on ω,
- $< \overline{v^2(\omega)} >$ is the mean square velocity of the housing.

with:

$$< \overline{v^2(\omega)} >= \frac{1}{S}\int_s (\frac{1}{T}\int_{-T/2}^{-T/2} v^2(M,\omega,t)dt)dS \quad (34)$$

Finally, the acoustic power in decibel is:

$$L_w(dB) = 10\log_{10}(\frac{W_{ac}}{W_{ref}}) \quad (35)$$

with $W_{ref} = 10^{-12}$ W.

The computation of the radiation factor of a structure is complex. A simplifying assumption is thus used: above a critical frequency f_c, one may consider the acoustic radiation factor equal to 1. The critical frequency f_c is equal to:

$$f_c = \frac{c_0^2}{2\pi}\sqrt{\frac{12\rho_0(1-\nu^2)}{Eh^2}} \quad (36)$$

where,

- E is the Young Modulus,
- ν is the Poisson coefficient,
- h is the housing thickness.

For the studied planetary gear set, f_c is of the same order of magnitude as the mesh frequency (1080 Hz at the maximum input speed 3000 rpm), so that the dynamic response harmonics are highter than this critical frequency. Therefore, the acoustic power can be estimated from the dynamic response of the housing.

Numerical results

In the following section, the complete procedure presented in this paper is applied on the planetary gear set presented previously.

Static transmission errors and dynamic transmission errors

The planetary gear is considered at its design stage: gear teeth without profile correction and manufacturing error are assumed. The STE and mesh stiffness fluctuations only depend on gears macro-geometry, teeth deflection induced by applied load and fluctuation of the number of teeth simultaneously in contact. The STE and the mesh stiffness's fluctuation are computed for an output torque equal to 100 N.m. Figure 4a displays the differents STE computed. Their fluctuations show rectangular wave form as expected for a spur gear with perfect micro-geometry. Moreover, the Fourier Transform of such signal shows numerous harmonics. The STE spectra in Figure 4b shows that the sixth harmonic (H6) amplitude is about one fifth of the first harmonic (H1). The mean value of ring-planet STE is lower than the sun-planet one, resulting on higher mesh stiffness mean values. Indeed, the ring gear is directly machined in the thick housing, leading to a stiff system.

For a perfect axisymmetric housing and identical stiffness's, the energetic contribution of eigenmodes should be the same for all sun gear/planet meshes and planet/ring gear meshes. The finite element model keeps the actual not perfectly axisymmetric geometry. However, Figure 5 shows that all sun gear/planet meshes have a similar behavior as well as all planet/ring gear meshes. Critical modes are observed near 6300 Hz for sun gear/planet meshes and near 8300 Hz for planet / ring gear meshes So that, the axisymmetry of the housing assumption can be validated.

Figure 6 displayd amplitude of dynamic transmission errors (DTE) versus mesh frequency. A peak at 6300 Hz is observed for sun gear/planet meshes (see Figure 6a). It corresponds to the resonant excitation of the critical modes by the first harmonic of the mesh frequency, which is the main excitation component as shown in STE spectra displayed on Figure 4b. The DTE has a smoother form for the planet/ring gear meshes (see Figure 6b). Indeed, the first harmonic STE spectra does not have a level that stands out the others, as shown in 4b. The maximum amplitude of DTE is observed at 2100 Hz. It corresponds to the excitation of the critical modes near 8300 Hz by the fourth harmonic of the mesh frequency and the critical modes near 6300 Hz by the third harmonic of the mesh frequency. The dynamic transmission error display Figure 6c correspond to the sum of contributions of the dynamic transmission errors $(e_1 + e_4)$, $(e_2 + e_5)$ and $(e_3 + e_6)$ and are mainly induced by sun gear/planet meshes excitations.

[Insert Figures 4 5 6]

Dynamic response of the housing

Figure 7 displays the waterfall acceleration of a point localized on the housing surface. The vibratory state of the housing shows the multi-harmonics components, which is typical of whining noise problems. Another phenomenom is observed: the energy is not concentrated only on mesh frequency harmonics. Some sidebands are also observed because of the carrier rotation. Few sidebands occur (see the waterfall zoom on Figure 7) because the simulation is performed for perfect gears. Based on Inapolat and Kahraman[20] observations, the consideration of dissimilar manufacturing errors for each planets should lead to the arising of more numerous sidebands. The waterfall is consistent with previous observation. The resonant excitation of critical modes previously identified (6300 Hz and 8300 Hz) by the harmonics of mesh frequency is observed.

The figure 8 displays the total acoustic power versus the input speed. The level is about 65 dB for input speeds larger than 1100 rpm. Indeed, the waterfall displays Figure 7 shows that beyond this speed, the resonant excitation of critical modes previously identified (6300 Hz and 8300 Hz) occurs.

[Insert Figures 7 8]

From the static transmission errors to the housing vibration state, the simulation needs less than a hour, including finite elements modal basis computation and signal modulation, with a personal computer (processor i7-3740QM 2.7 GHz and 8 Go RAM)

Conclusion and perspectives

This paper presents a complete method to predict the whining noise emitted by a planetary gear set resulting from the STE and mesh stiffness fluctuations. The STE and the load distribution along the multiple contact lines are computed by solving equations of contact at all the meshes simultaneously. Tooth compliance and ring gear elasticity are taken into account. Tooth manufacturing errors and profile corrections can be also be taking into account. The meshes stiffness's fluctuations are then deduced. The corresponding mean values are introduced in the finite element modelling of the planetary gear set in order to compute its modal basis. Finally, the modal equations of motion are solved in the frequency domain using a spectral iterative method allowing fast computation of the stationary dynamic response of parametric systems. Dynamic transmission errors for sun gear/planet meshes and for planet/ring gear meshes, as well as the dynamic response at any degree of freedom of the discretized model. Finally, the whining noise is evaluated from the housing vibratory state and the acoustic power.

Few experimental tests on planetary gears are available in the literature, because of their geometry and complex kinetics. The need to demonstrate the validity of the numerical models developed has led to a series of experimental measurements, from which the waterfall of the acceleration response of a housing displayed in Figure 9 is derived. The comparison shows good correlation between the measurement and the simulation. Indeed, it shows the ability of the numerical model to catch the resonant excitation of critical eigenmodes. However, some vibratory level discrepancies are observe because gear teeth without profile correction and manufacturing error are assumed for the simulation performed. At last, future comparisons between simulation and measurement will include actual boundary conditions of the planetary gear set with the test bench, tuning of the global modal basis, STE correlation with the actual micro-geometry errors and corrections to ensure better comparison.

[Insert Figure 9]

The proposed method is an efficient tool to predict the dynamic response ans the whining noise of a planetary gear set, as long as the modal basis does not depend on planets position during operation. Short computational time makes possible to use this method early in the design process as an optimization tool. Moreover, this method can be applied on actual systems (without any geometry simplification) including boundary conditions, leading to representative simulation. However, some housing design can shows larger geometric variations. Effect of the moving contacts coupled with the variation of the ring thickness is a work in progress.

Acknowledgements

This work has been performed within the LabCom LADAGE (LAboratoire de Dynamique des engrenAGEs) created by the LTDS and Vibratec and funded by the French National Research Agency / ANR under the reference number ANR-14-LAB6-0003.

The authors are also members of the Labex CeLyA of Université de Lyon, operated by the French National Research Agency (ANR-10-LABX-0060 / ANR-11-IDEX-0007)

References

1. Cooley CG and Parker RG. A review of planetary and epicyclic gear: dynamics and vibrations research. *Applied Mechanics Reviews* 2014; 66: 040804.
2. Welbourn DB. Fundamental knowledge of gear noise - a survey. *Proceedings of conf on Noise and Vibration of Engines and Transmissions* 1979; C177/79: 9–29.
3. Harris SL. Dynamic loads on the teeth of spur gears. *Proceedings of the Institution of Mechanical Engineers* 1958; 172(1): 87–112.
4. Gregory RW, Harris SL and Munro RG. Dynamic behaviour of spur gears. *Proceedings of the Institution of Mechanical Engineers* 1963; 178: 207–218.
5. Rigaud E and Barday D. Modelling and analysis of static transmission error - effect of wheel body deformation and interactions between adjacent loaded teeth. *4th World Congress on Gearing and Power Transmission* 1999; 3: 1961–1972.
6. Tavakoli MS and Houser DR. Optimum profile modifications for the minimization of static transmission errors of spur gears. *Journal of Mechanism Transmission and Automation in Design* 1986; 108(1): 86–94.
7. Hu Y, Talbot D and Kahraman A. A load distribution model for planetary gear sets. *Journal of Mechanical Design* 2018; 140: 053302–053302–14.
8. Bodas A and Kahraman A. Influence of carrier and gear manufacturing errors on the static load sharing behavior of planetary gear sets. *JSME International Journal Series C* 2004; 47: 908–915.
9. Ligata H, Kahraman A and Singh A. A closed-form planet load sharing formulation for planetary gear sets using a translational analogy. *Journal of Mechanical Design* 2009; 131(2): 021007.
10. Leque N and Kahraman A. A three-dimensional load sharing model of planetary gear sets having manufacturing errors. *Journal of Mechanical Design* 2017; 139(3): 033302.
11. Lin J and Parker RG. Analytical characterization of the unique properties of planetary gear free vibration. *Journal of Vibration and Acoustics* 1999; 121: 316–321.
12. Abousleiman V and Velex P. A hybrid 3d finite element/lumped parameter model for quasi-static and dynamic analyses of planetary/epicyclic gear sets. *Mechanism and Machine Theory* 2006; 41: 725–748.
13. Perret-Liaudet J. An original method for computing the response of a parametrically excited forced system. *Journal of Sound and Vibration* 1996; 196(2): 165–177.
14. Carbonelli A, Rigaud E and Perret-Liaudet J. Vibro-acoustic analysis of geared systems — predicting and controlling the whining noise. *Automotive NVH Technology, Editors Fuchs A,*

Nijman E, Priebsch H-H, SpringerBriefs in Applied Sciences and Technology, Springer International Publishing 2016; : 63–79.

15. Neufond J, Xu Y, Perret-Liaudet J et al. The iterative spectral method for computing the planetary gear dynamic response. *Proceedings of VDI International Conference on Gears, 2017* 2017; 2294-1: 209–218.
16. Rigaud E, Sabot J and Perret-Liaudet J. Approche globale pour l'analyse de la réponse vibratoire d'une transmission par engrenage. *Revue Européenne des Eléments Finis* 2000; 9: 315–330.
17. Parker RG and Lin J. Mesh phasing relationships in planetary and epicyclic gears. *Journal of Mechanical Design* 2004; 126(2): 365–370.
18. Tsai SJ, Huang GL and Ye SY. Gear meshing analysis of planetary gear sets with a floating sun gear. *Mechanism and Machine Theory* 2015; 84: 145–163.
19. Rigaud E and Sabot J. Effect of elasticity of shafts, bearings, casing and couplings on the critical rotational speeds of a gearbox. *VDI Berichte* 1996; 1230: 833–845.
20. Inalpolat M and Kahraman A. A theoretical and experimental investigation of modulation sidebands of planetary gear sets. *Journal of sound and vibration* 2009; 323: 677–696.

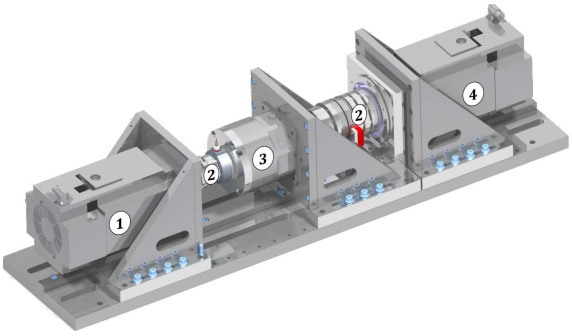

Figure 1. Test bench: (1) electric motor, (2) couplings, (3) planetary gear set, (4) brake

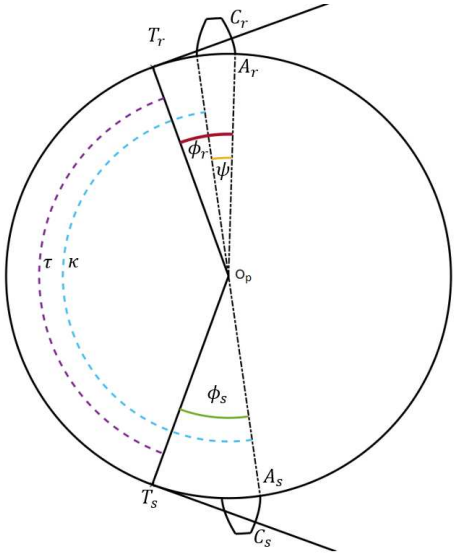

Figure 2. Angles involved in the determination of the computation of the abscissa of contact of the planet/ring gear meshes: ϕ_s : —, ϕ_r: —, ψ: —, τ: - -, κ: - -

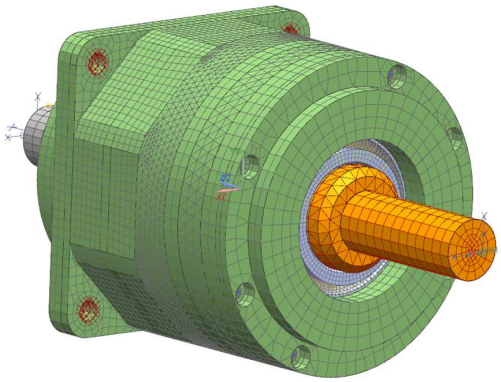

Figure 3. Finite element model of the planetary gear set

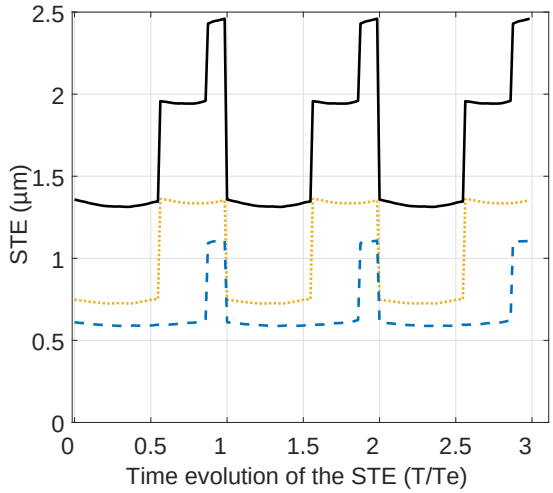

(a) Time evolution of the STE: ·· sun gear/planet STE δ_1, δ_2 and δ_3; -- planet/ring gear STE δ_4, δ_5 and δ_6; — Δ

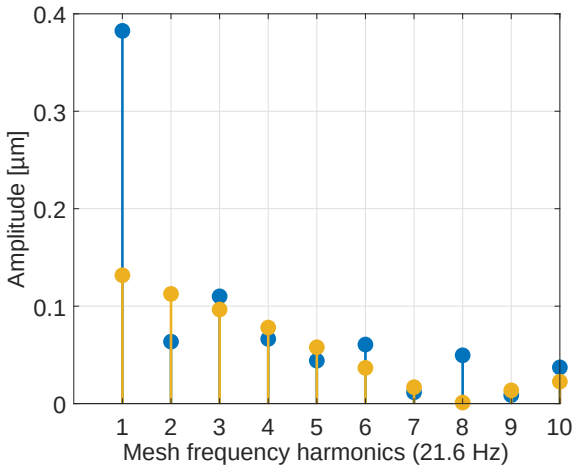

(b) STE spectra: sun gear/planet STE δ_1, δ_2 and δ_3 —● and planet/ring gear STE δ_4, δ_5 and δ_6 —●)

Figure 4. Static transmission errors

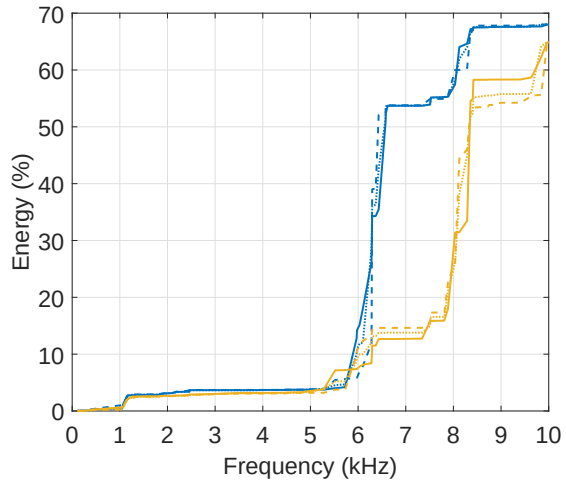

Figure 5. Added-up energy contribution of eigenmodes: — sun gear/planet 1 mesh; -- sun gear/planet 2 mesh; ·· sun gear/planet 3 mesh; — planet/ring gear 1 mesh; -- planet/ring gear 2 mesh; ·· planet/ring gear 3 mesh

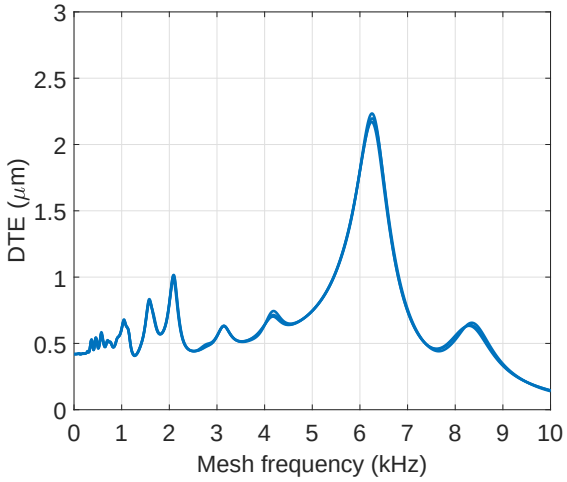

(a) Dynamic transmission errors for sun gear/planet meshes (e_1, e_2 and e_3)

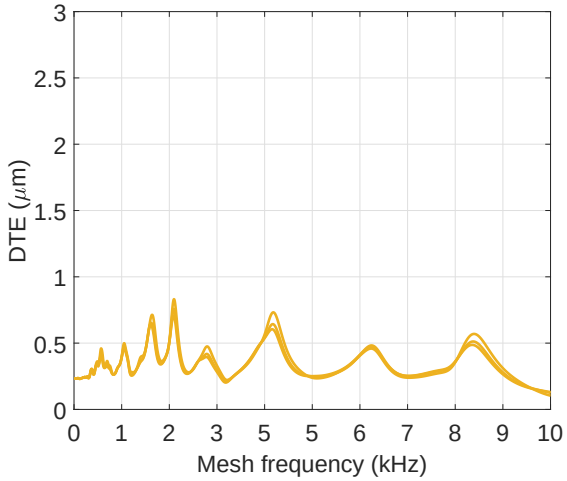

(b) Dynamic transmission errors for planet/ring gear meshes (e_4, e_5 and e_6)

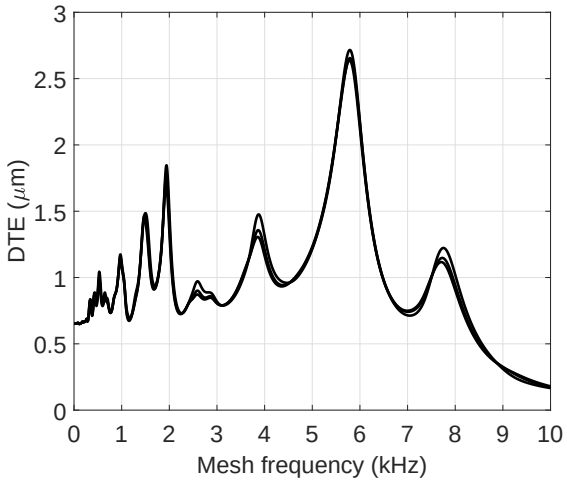

(c) Sum of dynamic transmission errors ($e_1 + e_4$, $e_2 + e_5$ and $e_3 + e_6$)

Figure 6. Dynamic transmission errors

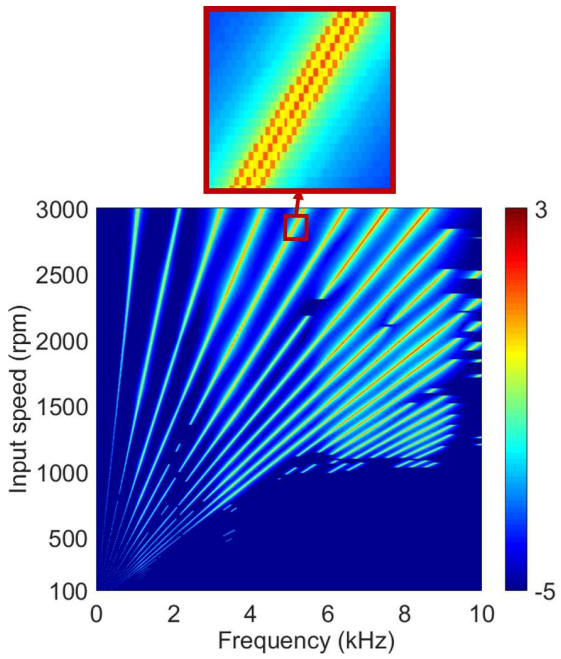

Figure 7. Waterfall of the acceleration response of a housing point localized on radial surface, numerical simulation

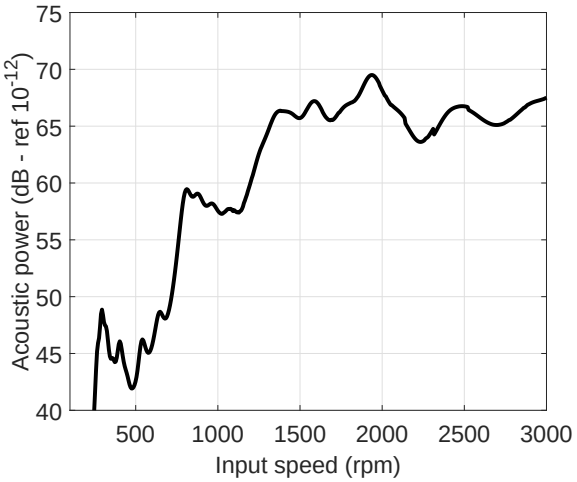

Figure 8. Acoustic power versus input speed

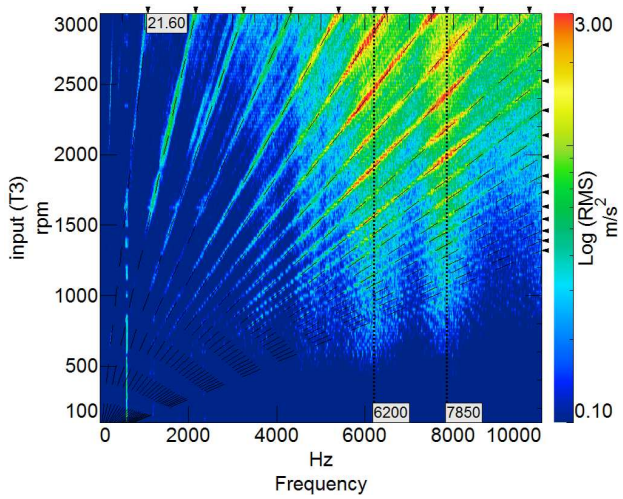

Figure 9. Waterfall of the acceleration response of a housing point localized on radial surface, experimental data